AGU PUBLICATIONS

JGR

Journal of Geophysical Research: Space Physics

RESEARCH ARTICLE
10.1002/2015JA021305

Key Points:
- These are the first reported ESWs observed in connection with Enceladus
- These are the first survey results of the location of ESWs observed near Saturn
- Characteristics of ESWs observed near Saturn are provided

Correspondence to:
J. S. Pickett,
pickett@uiowa.edu

Citation:
Pickett, J. S., W. S. Kurth, D. A. Gurnett, R. L. Huff, J. B. Faden, T. F. Averkamp, D. Píša, and G. H. Jones (2015), Electrostatic solitary waves observed at Saturn by Cassini inside 10 R_s and near Enceladus, *J. Geophys. Res. Space Physics*, *120*, doi:10.1002/2015JA021305.

Received 3 APR 2015
Accepted 29 JUL 2015
Accepted article online 1 AUG 2015

Electrostatic solitary waves observed at Saturn by Cassini inside 10 R_s and near Enceladus

J. S. Pickett[1], W. S. Kurth[1], D. A. Gurnett[1], R. L. Huff[1], J. B. Faden[1], T. F. Averkamp[1], D. Píša[1,2], and G. H. Jones[3,4]

[1]Department of Physics and Astronomy, University of Iowa, Iowa City, Iowa, USA, [2]Institute of Atmospheric Physics AS CR, Prague, Czech Republic, [3]Mullard Space Science Laboratory, Department of Space and Climate Physics, University College London, Dorking, UK, [4]Centre for Planetary Sciences at UCL/Birkbeck, London, UK

Abstract We have analyzed the Cassini Radio and Plasma Wave Science Wideband Receiver (WBR) data specifically looking for the presence of bipolar electrostatic solitary waves (ESWs). Typical examples of these ESWs are provided to show that when they are present, several of them may be detected over a few to several millisecond time span. We carried out an event study of an Enceladus encounter which took place on 9 October 2008. Approximately 30 min prior to and during the crossing of the Enceladus dust plume, several ESWs are observed with amplitudes of about 100 μV/m up to about 140 mV/m, and time durations of several tens of microseconds up to 250 μs. The highest amplitudes (over 10 mV/m) were observed only during the closest approach to Enceladus. We also carried out an ESW survey using the WBR for all years from 2004 to 2008 for distances less than 10 R_s. The survey clearly shows that most of the ESWs are found on the nightside, with a high percentage of them in the range of 4–6 R_s. This location is consistent with the densest part of Saturn's E ring and Enceladus' orbit. These are the first extended survey results of ESWs near Saturn and the first reported ESWs in connection with Enceladus. We discuss possibilities for the generation of these nonlinear ESWs, which involve current, beam, and acoustic, including dust, instabilities.

1. Introduction

Electrostatic solitary waves (ESWs), also sometimes described as electrostatic solitary structures in the literature, have been detected by spacecraft since the 1970s when they were first observed on the S3-3 mission in the Earth's auroral ionosphere in association with small-amplitude double layers [*Temerin et al*., 1982]. The solitary waves consisted of pulses in the electric field waveform data when the electric field sensors were aligned with the local magnetic field. *Dubouloz et al*. [1991] first proposed that the high-frequency part of the broadband electrostatic noise (BEN) observed in Viking measurements made in the dayside auroral zone could be electron acoustic solitons passing by the satellite. BEN, first identified by *Gurnett et al*. [1976] and *Gurnett and Frank* [1977], had been observed in the spectral data of several missions up to that point, being particularly prevalent at boundary layer crossings, along auroral field lines, and in turbulent regions, but had not been associated with solitary waves. *Matsumoto et al*. [1994] finally proved the association between electrostatic solitary wave pulses observed in the time domain and the broadband electrostatic noise observed in the frequency domain by transforming their high time resolution waveform measurements of ESWs obtained on Geotail using the fast Fourier transform. However, *Matsumoto et al*. [1994] found that these ESWs differed from the solitons observed on Viking in that they were isolated bipolar pulses with no internal structure and were electrostatic in nature with no observed corresponding magnetic component. They proposed a nonlinear Bernstein-Greene-Kruskal (BGK) potential model [*Bernstein et al*., 1957; *Chen and Parks*, 2002] for generation of the ESWs.

There have been numerous published studies using data from several spacecraft (Geotail, Polar, Wind, FAST, Cluster, and THEMIS) showing ESWs detected around Earth in all of its boundary layers, in turbulent regions, in magnetic reconnection diffusion regions, and in the near Earth solar wind since the initial Geotail observations. Many of these are cited in the introductions to *Lakhina et al*. [2011], which discusses ESWs in the plasma sheet boundary layer, and *Li et al*. [2014], which deals with ESWs associated with the separatrix of magnetic reconnection in the near-Earth current sheet. Some of these reports show propagation of the ESWs from one antenna probe to another on a single spacecraft, such as on Polar [*Franz et al*., 1998] and FAST [*Ergun et al*., 1998a], over distances up to ~100 m. Using waveform measurements on two Cluster spacecraft, *Pickett et al*.

[2004a, 2010] showed the propagation of ESWs from one spacecraft to another over distances of several kilometers, thus demonstrating the stability of some ESWs.

ESWs have also been detected at Saturn [*Williams et al*., 2006], in the wake of Jupiter's moon Europa [*Kurth et al*., 2001a], in the lunar wake of Earth's Moon [*Hashimoto et al*., 2010], and at an interplanetary shock [*Williams et al*., 2005].

Recently, ESWs and spiky electric field structures associated with electron holes and double layers have been observed in the Earth's outer radiation belts by the Van Allen Probes [*Mozer et al*., 2013, 2014; *Malaspina et al*., 2014]. These structures have been shown to be important for relativistic electron acceleration and precipitation that generates auroras. Acceleration mechanisms of this type may also be important in the planetary radiation belts of the outer gas giant planets, including Saturn [*Mozer et al*., 2014].

As noted above, ESWs are identified in the electric field waveform data as pulses. Ideally, these pulses are half-sinusoids of one sign followed by half-sinusoids of the oppose sign and isolated either in time or in amplitude from other wave activity. These have been termed bipolar pulses. Other types of pulses which have only a half-sinusoid of either sign (monopolar pulses), and three half-sinusoids with two of one sign and one of the other (tripolar pulses) when aligned with the magnetic field, are usually interpreted as double layers because a potential change is observed across them. Monopolar pulses have also been interpreted as the perpendicular component, to the magnetic field, of bipolar pulses that are detected along a magnetic field line by a set of electric field antennas [*Franz et al*., 1998].

Some ESWs observed near Earth have been found to have magnetic components perpendicular to the background magnetic field, e.g., *Mozer et al*. [1997] and *Tsurutani et al*. [1998] using Polar waveform data and *Ergun et al*. [1998b] using FAST waveform data. However, an analysis by *Ergun et al*. [1998b] of these high time resolution magnetic components obtained simultaneously with the electric components led to the conclusion that they were the result of the Lorentz field, indicating that the pulses were indeed electrostatic in their frame of reference. *Andersson et al*. [2009], using THEMIS waveform data obtained in Earth's plasma sheet, reported the first 3-D observations of magnetic field perturbations caused by electron holes, including the detection of a $\delta B_{\parallel}$ signal. The electron holes were detected as bipolar electric field signals ($\delta E_{\parallel}$) parallel to B_0. The electron holes associated with $\delta B_{\parallel}$ have features that distinguish them from earlier observations, in particular larger electric fields ($\delta \mathbf{E} \sim O(100\ \mathrm{mV/m})$), high speeds, large parallel sizes, moderate to strong center potentials, and elongated shapes. These features are similar to those associated with magnetic reconnection observed in laboratory measurements.

Several theoretical and modeling studies have led to the conclusion that ESWs are generated by current, beam, and acoustic instabilities. See the introduction to *Lakhina et al*. [2011] for a review of some of these studies. When generated out of current and beam instabilities, these ESWs usually represent potential structures (electron or ion phase space holes). When generated out of acoustic instabilities, they primarily represent density structures. As noted by *Lakhina et al*. [2011], historically, most studies have tended to discount the acoustic instability as the active generation process of ESWs observed in space since classical Korteweg–de Vries-type solitons do not fit the width-amplitude relationship reported for ESWs observed in space. However, the arbitrary amplitude weak solitons as predicted by the models based on the Sagdeev pseudo-potential techniques can either increase or decrease depending on the width of the soliton and depending on the parametric range used [*Ghosh and Lakhina*, 2004] and thus provide a promising alternative method for the generation of ESWs. *Chen et al*. [2003] and *Pickett et al*. [2005] have also suggested that ESWs can be generated spontaneously out of turbulence, the basis for which is provided, in part, by obtaining a continuum of parameter space for phase-space electron and ion holes (BGK solitary waves) [*Chen et al*., 2004].

In this study we only use data obtained by the Cassini Wideband Receiver (WBR), which is a part of the Radio and Plasma Wave Science (RPWS) instrument mounted on the Cassini spacecraft [*Gurnett et al*., 2004]. The WBR makes measurements of only one electric field component, using only the single dipole E_x antenna, which is 9.2 m in length, for the observations presented below. Thus, apart from noting the angle of the antenna to the measured magnetic field, there is no way to determine the ESW's velocity, or size, as has been done on several spacecraft, most notably Polar and FAST [*Franz et al*., 1998, 2005, *Ergun et al*., 1998a]. The WBR data were obtained with two different filter bandwidths, 10 kHz and 80 kHz, which enable the capture of ESWs with different time scales, i.e., the wider the filter bandwidth, the shorter the time scale that can

be observed. The sampling rate of the WBR in the 10 kHz mode is 27,777 samples per second, with a resolution of 36 μs between samples, and 222,222 samples per second in the 80 kHz bandwidth, with a resolution of 4.5 μs between samples. Thus, these high sampling rates allow structures to be resolved to as short as a few tens of microseconds with the 80 kHz bandwidth and down to a few hundreds of microseconds with the 10 kHz bandwidth.

The WBR electric field measurements are obtained by using a pair of elements as a dipole antenna (E_x). The measured signal is the difference in voltage between the two elements. The WBR data are then calibrated as described in Chapter 12 of the Cassini RPWS Instrument Calibration document, which is archived at the Planetary Plasma Interactions node of NASA's Planetary Data System (http://ppi.pds.nasa.gov/archive1/CORPWS_0193/DOCUMENT/RPWSCAL/). All calibrated differential voltage amplitudes reported here have been multiplied by the square root of 2 in order to account for the fact that the calibrations as described are carried out with V_{RMS} required to obtain a frequency spectrum. The obtained voltages are then divided by the dipole antenna length, 9.26 m, which is the distance between the two midpoints of the elements. Finally, a correction is applied to account for the 8 dB loss associated with the capacitive voltage division. Because the WBR measures only one component of the electric field, the amplitudes of the ESWs could be larger than the values stated in sections 2 and 3.

Because of the multipole filters incorporated in the WBR, pulses longer than an experimentally determined value for each of the bandwidths will be distorted. This is ~250 μs for the 80 kHz bandwidth and 1 ms for the 10 kHz bandwidth based on bench tests of a spare WBR. Since the Cassini WBR results have not been published, the reader is referred to *Swanner et al*. [2006] for the results of similar pulse distortion tests conducted on the spare Cluster WideBand Data (WBD) receiver, which is very similar in design to the Cassini WBR. The ESW data obtained by the WBR during its Earth flyby in 1999 [*Kurth et al*., 2001b] were compared to observations by other spacecraft, most notably those of the Cluster WBD. The Cassini ESWs were very similar in amplitude and time duration for specific plasma regions, thus providing confidence that Cassini ESWs have been properly analyzed and interpreted.

The WBR does not make concurrent measurements of the magnetic field with its measurements of the electric field nor does any other wave receiver on Cassini make such magnetic waveform measurements in the required frequency range. Therefore, we are unable to state with certainty that the observed bipolar pulses observed with the WBR are electrostatic. However, as noted in *Williams et al*. [2006], who reported the first observations of ESWs at Saturn, they examined the waveform receiver (WFR) data, which measure the vector magnetic field, at times when bipolar pulses were observed in the electric field waveforms. They detected no evidence of magnetic components, so by extension they assumed that the bipolar pulses observed by the WBR were likewise electrostatic. Furthermore, the electric field amplitudes of the bipolar pulses observed by the WBR at Saturn, as will be shown in the next sections, are usually not of the order of those observed by *Andersson et al*. [2009] in the Earth's plasma sheet, which had significant magnetic fields parallel to B_0. For this reason and because all earlier observations of bipolar pulses with magnetic components perpendicular to B_0 were consistent with the Lorentz field and thus electrostatic in their frame of reference, we assume that most, if not all, of the ESWs reported here are electrostatic as well.

Below we provide two examples of typical ESWs observed by the WBR at Saturn. This is followed by a focused ESW event study of data obtained on 9 October 2008 during the E5 Enceladus encounter on the nightside of Saturn near 4 R_s where ESWs are observed in abundance. It is followed by a survey showing where ESWs are detected inside 10 R_s for the period from orbit insertion in 2004 through 2008. The last section contains a discussion of the results and the conclusions drawn from the study.

2. Typical ESWs

Examples of typical ESWs observed by Cassini are shown in Figures 1 and 2. Figure 1 presents a ≃74 ms WBR snapshot showing a series of several ESWs observed on 16 January 2005 using the narrower 10 kHz filter bandwidth when the spacecraft was located at 8.4 R_s, −3.1° latitude (lat.) and 0100 magnetic local time (MLT). For reference, the time duration (0.4 ms) and amplitude (0.338 mV/m) of one of these ESWs, identified by the black arrow, are provided in the figure. Although there is a little variation in the amplitudes of the various ESWs, they are not significantly different one from another. Their time durations are all on the order

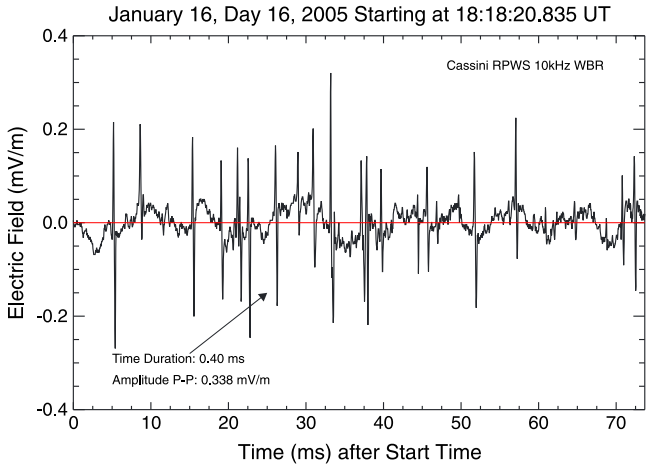

Figure 1. Time series data of the calibrated electric field data over a ≃74 ms interval from the Cassini RPWS WBR, 10 kHz filter bandwidth, obtained on 16 January 2005. These data show several bipolar ESW pulses embedded within a lower amplitude oscillatory wave. The amplitude and time duration of one of the pulses in the snapshot, identified by the black arrow, are provided.

of a few hundreds of microseconds. One significant aspect to these ESW bipolar pulses is that they all have initial positive electric fields, followed by negative. ESWs observed with opposite initial field directions in such short time periods would usually imply that the ESWs are propagating in opposite directions or that they are of opposite potential.

Figure 2 is an example of some ESWs that were obtained with the wider 80 kHz bandwidth filter on 9 October 2008. Five well-defined bipolar ESWs are observed during this ≃7 ms WBR snapshot. Because of the wider bandwidth, we observe that the time duration of most of the ESWs is now shorter, on the order of several tens of microseconds. Pulses of this time scale could not have been resolved with the narrower bandwidth. We find that the amplitudes are similar in that they are on the order of a few tenths of mV/m. Once again, all of the pulses have the same initial field direction, in this case negative, implying that they are probably propagating past the spacecraft in the same direction.

3. Event Study of 9 October 2008

We now investigate an ESW event that occurred on 9 October 2008 when the spacecraft was located on the nightside around 4 R_s and crossing the equator from north to south. Figure 3 presents data from this event during which time the RPWS WBR was in the 80 kHz filter bandwidth mode. An electric field frequency-time spectrogram of the WBR data is provided in Figure 3e, with color providing the spectral density of one electric field component. For reference, the waveform data shown in Figure 2 were Fourier transformed and are included as one frequency/time slice in this spectrogram. Ephemeris data are provided below Figure 3e: distance from the center of Saturn in R_s, longitude (lon), and latitude (lat). Initially, the WBR data show the presence of BEN, which is observed to extend from the smallest frequency measured up to around 40 kHz and which is typically the fast Fourier transform signature of impulsive emissions such as ESWs and dust impacts. During this time, narrowband upper hybrid frequency emissions are seen starting from around 30 kHz and continually rising to about 80 kHz around 19:00 UT, and then steadily decreasing after 19:10 UT. Also, above this frequency we observe early on a type of emission similar to escaping continuum observed at Earth [*Gurnett*, 1975; *Kurth et al.*, 1981]. In addition,

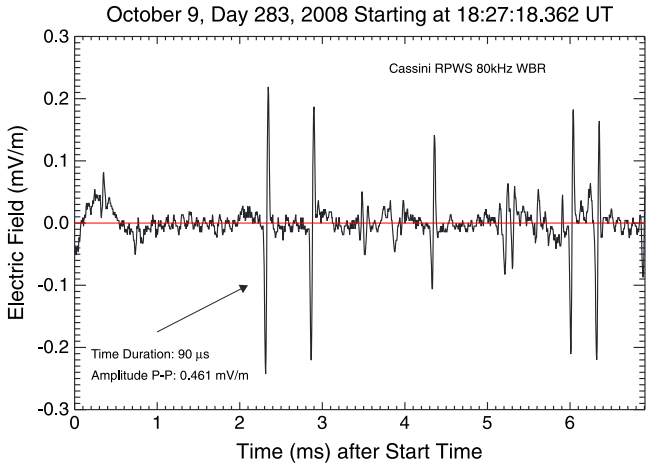

Figure 2. Time series data of the calibrated electric field data over a ≃7 ms interval from the Cassini RPWS WBR, 80 kHz filter bandwidth, obtained on 9 October 2008, ~0.5 h before crossing the Enceladus dust plume. These data show five well-defined bipolar ESW pulses embedded within a much lower amplitude oscillatory wave. Note that the amplitudes of these ESWs are comparable to those in Figure 1, but their time durations are much shorter.

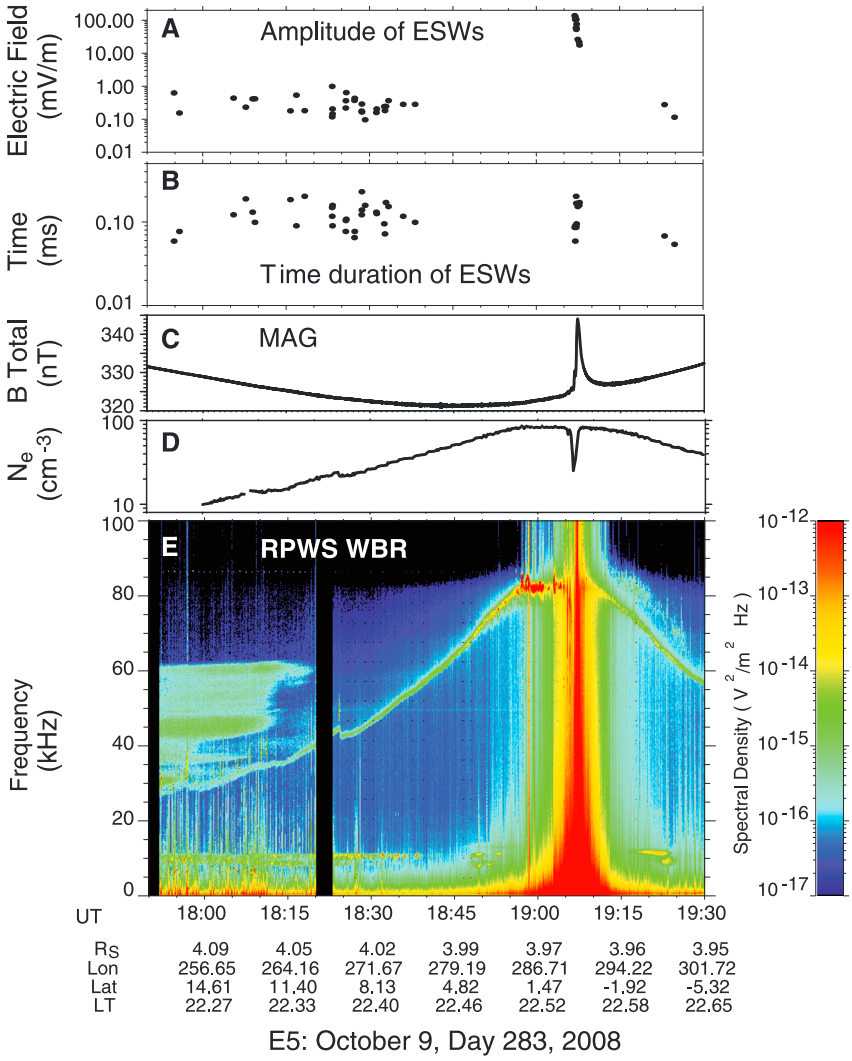

Figure 3. Cassini data obtained on 9 October 2008 over a 35 min period during an Enceladus encounter (E5). (a) The amplitude, in mV/m, of detected ESWs (black dots) obtained through analysis of the Cassini RPWS WBR data. (b) The time scale, in ms, of those same ESWs, consisting of the time duration from the start of the bipolar pulse to the end of it. (c) The total measured magnetic field from the MAG instrument, given in nT. (d) The electron density obtained from the observed upper hybrid resonance frequency. (e) The electric field frequency-time spectrogram of observed waves, the data having been obtained by the Cassini RPWS WBR. The spectral density, in $V^2\,m^{-2}\,Hz^{-1}$, is given by the color scale on the right with frequency, in kHz, given by the vertical axis.

two sets of nearly constant frequency bursty waves are seen at approximately 9–11 kHz from 17:50 to 18:40 UT. The lower frequency set of bursty waves decreases slightly in frequency in concert with the decrease in the magnetic field and are most likely electron cyclotron waves. The other set of bursty waves rises slightly in frequency during this same period of time and thus are probably not locally generated electron cyclotron waves.

Around 19:00–19:20 UT, the Enceladus dust plume is encountered with closest approach to Enceladus occurring at 19:06:40 UT at 25 km altitude. During this Enceladus crossing (E5), there is the usual extremely intense broadband noise extending through the entire frequency range of the WBR. Most noise of this type has been found to be associated with dust impacts [*Ye et al.*, 2014] on the spacecraft and antenna. As shown in Figure 4, the waveform pulses associated with these dust impacts have a different appearance than those of ESWs. The top plot of Figure 4 shows a ≃7 ms WBR snapshot taken during the time of closest approach to Enceladus. Three waveforms have been highlighted during this period: an ESW in A, the light blue box; a dust impact in B, the light orange box; and an oscillatory dust impact in C, the light green box. Each of these waveforms

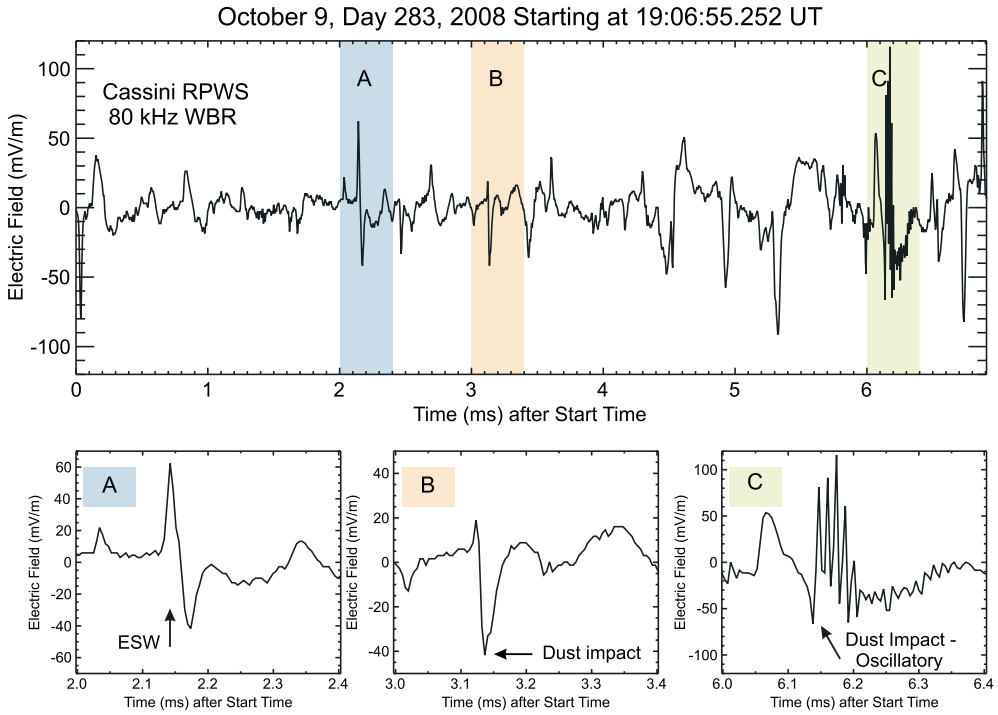

Figure 4. WBR waveforms obtained during Enceladus encounter E5. Top: ≃7 ms WBR snapshot highlighting three types of waveforms with expanded views provided in plots A, B, and C according to the color code. A: ESW pulse showing the bipolar nature of nearly symmetric negative and positive peaks, p-p amplitude of ~103 mV/m, and pulse time duration of 80 μs. B: Dust impact signature consistent with dust impacting the spacecraft. C: Oscillatory dust impact signature consistent with ringing at the plasma frequency.

is shown in higher time resolution in the three individual plots shown below the ≃7 ms WBR snapshot. Dust impact pulses have a very fast risetime and a longer relaxation time than ESWs, usually resembling the ringing of a filter, as shown in the sample B waveform. The bipolar ESWs have a much more symmetric waveform as shown in the sample A waveform. Dust impacts sometimes have an oscillatory behavior as shown in the sample C waveform, the oscillation being consistent with, or close to, the local plasma frequency [*Ye et al*., 2014]. For reference, similar ESW and dust impact waveforms as shown in space observations have been observed in the laboratory by *Lefebvre et al*. [2011] and *Lee et al*. [2012], respectively.

Figure 3c shows the total magnetic field measured by the magnetometer (MAG) instrument [*Dougherty et al*., 2004] for this event. The magnetic field shows no significant variation from what would be expected as the spacecraft approaches close to Saturn at 4 R_S. However, there is a significant increase in the field magnitude at closest approach to Enceladus which peaks around 19:07:15 UT. This increase is associated with the spacecraft crossing the Enceladus dust plume. The MAG data showing the individual magnetic field components in an Enceladus Interaction Coordinate System [*Dougherty et al*., 2006] for this E5 crossing is provided in Figure 3c of *Jones et al*. [2009]. The *X* component in this system is aligned with the corotational flow, with *Y* positive toward Saturn. Analysis of the *X* and *Z* components shows that there is initially a northward current up to 19:07:15 UT, followed by a southward current from 19:07:15 to 19:07:30 UT. The change in the magnetic field is due to the interaction with Enceladus as observed on similar Enceladus encounters prior to this one [*Dougherty et al*., 2006; *Jones et al*., 2009]. The magnetic field perturbation was found to be consistent with local outgassing, which was attributed to a plume from the surface of Enceladus near its south pole [see *Dougherty et al*., 2006, and references therein]. The plume's primary constituents were found to be water vapor [*Hansen et al*., 2006] and icy grains [*Spahn et al*., 2006] [see also *Jones et al*., 2009, and references therein].

The electron density for this event is presented in Figure 3d. The density is obtained from the RPWS low rate spectral data from the analysis of the upper hybrid resonance frequency, which is observed in the RPWS data of Figure 3e and which was discussed above. These data show that the electron density gradually rises as the spacecraft approaches Enceladus and decreases in a like manner as the spacecraft recedes from the moon.

However, at closest approach to the moon, when the magnetic field makes a dramatic and substantial increase over the period of approximately 2 min, the density undergoes a similar substantial decrease, indicating it is traversing a localized density cavity near Enceladus.

Analysis of the WBR waveform data for this E5 Enceladus encounter event is shown in Figures 3a and 3b. An automated program was used to find the bipolar ESWs using routines first developed by *Williams et al*. [2005, 2006]. After possible ESWs were identified in the data, the plots of these data were manually inspected to select only valid bipolar ESWs that were not distorted by the filters. For the event shown in Figure 3, and in general, for the survey provided in the next section, the time of the beginning of each WBR snapshot was recorded. These snapshots could contain one or more ESWs as evidenced by Figures 1 and 2. The properties of these ESWs were recorded in a separate file, consisting of the peak-to-peak amplitude and the time duration of each ESW pulse. These data were then plotted versus time as shown in Figures 3a and 3b, where a black dot represents a single detection. If more than one ESW was identified in a snapshot, only the mean values of the amplitude and time duration of all ESWs contained in that snapshot were plotted.

As shown in Figures 3a and 3b, bipolar ESW pulses are detected primarily in the period up to about 18:40 UT, associated with some of the BEN observed in Figure 3e. For completeness, we note that some of the BEN in this time period is also associated with dust impact pulses. In general, the frequency extent shown in Figure 3e is controlled by the time duration of the pulse, so the shorter the pulse time duration, the greater the frequency extent. These ESWs have amplitudes on the order of 100 μV/m up to about 140 mV/m and time durations of several tens to a few hundreds of microseconds. Any ESW time durations longer than 250 μs were discarded due to possible distortion as mentioned above. During the Enceladus plume encounter, however, we observe that the amplitudes of the detected ESWs are at least 2 orders of magnitude greater than those observed up to 18:40 UT and following the Enceladus plume encounter after 19:15 UT even though the time durations are quite comparable. However, during this time, the gain of the WBR has been greatly reduced so that only those ESWs with large amplitudes, on the order of the dust impacts, would be able to be resolved, whereas lower amplitude ESWs as were seen earlier in Figure 3 would not be detectable in the waveforms. In section 5 we will discuss the possibility that these higher-amplitude ESWs are specifically associated with the environment near Enceladus.

Although not shown here, the ESWs observed in Figures 3a and 3b were taken when the angle between the antenna making the measurement was within 40° of the magnetic field. The period of time from about 18:10 to 18:15 UT is a time in which this angle transitions from around 50° to 110° due to a spacecraft maneuver. During this time, no bipolar ESWs were detected.

4. ESW Survey

An ESW survey was carried out using Cassini RPWS WBR waveform data obtained after orbit insertion in July 2004 through 2008. The results of that survey are contained in Figure 5. Figure 5a is a polar coordinate map containing the WBR coverage in terms of number of WBR snapshots (both in 10 and 80 kHz filter bandwidth modes) scaled by the color bar, as a function of radial distance R, in Saturn radii (R_s) as the radial component, and magnetic local time (MLT), in hours, as the azimuthal component, in bins of 1 R_s by 1 h MLT for all latitudes. Bins colored black indicate that there are no WBR snapshots in those bins. In this figure we see that the coverage over the ~4 years of the survey is nearly uniform with the exceptions of increased coverage at (1) MLTs of 20–24 at distances less than 7 R_s, (2) 22 MLT at distances of 3–5 R_s associated with Enceladus encounters, and (3) MLTs of dawn to noon, with dust in the ring plane and chorus waves being particularly targeted near equator crossings.

Figure 5b uses the same coordinate system as Figure 5a, but instead of total WBR coverage, contains the ESW distribution as a percentage of the number of WBR snapshots containing ESWs in any particular bin to the total number of WBR snapshots contained in that bin. Bins colored white indicate that there are no ESWs detected in those bins. Although ESWs are not particularly numerous as shown by the percentages on the color bar, there is clearly a preference for them to be located on the nightside inside 10 R_s (the survey did not include distances greater than 10 R_s for the reasons provided in the next section). We point out that many ESWs were detected at 4–6 R_s, which includes the expected Enceladus encounters.

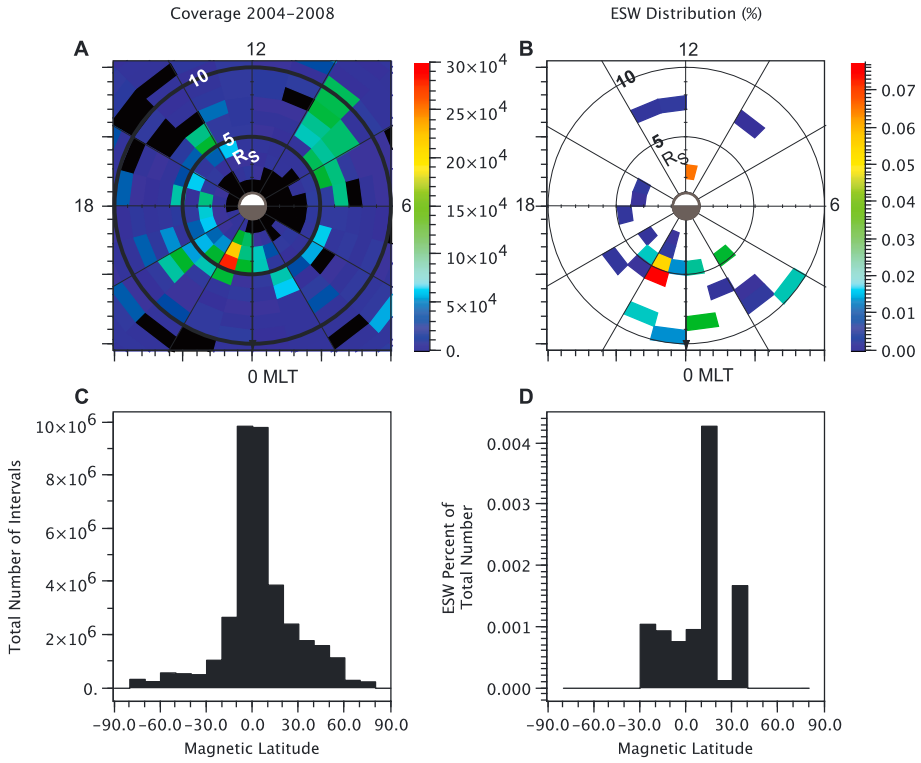

Figure 5. Results of the ESW survey for the years 2004 through 2008 while Cassini was in orbit around Saturn. The survey was restricted to distances less than 10 R_S. (a) The overall coverage for the Cassini RPWS WBR in the 10 and 80 kHz bandwidth modes. The polar map provides distance, in R_S, as the radial component and MLT, in hours, as the azimuthal component, with color providing the total number of WBR snapshots contained within each 1 R_S by 1 hr MLT bin. (b) The results of the ESW detections for the same parameter space as in Figure 5a presented as a percent of the total WBR snapshots per bin. (c) A histogram that provides the number of WBR snapshots contained in each 10° wide latitude bar. (d) A histogram showing ESW detections as a percent of the total number of WBR snapshots for each 10° wide latitude bar.

Figure 5c is a histogram of the total number of WBR snapshots for the survey period versus the magnetic latitude north (positive) and south (negative) of the equator (0°), in 10° wide bins, at which they were obtained. As can be seen, the highest proportion falls near the magnetic equator, in line with E ring and chorus waves being particular targets for the WBR observations. Figure 5d shows the percentage of WBR snapshots in which ESWs were observed relative to total number of WBR snapshots obtained. A high percentage of the ESW detections are uniformly spread across southern latitudes up to 30°, in contrast to the northern latitudes where they are preferentially detected at 10–20° and 30–40°.

Although not shown in Figure 5, the Cassini orbit in 2006 and 2007 was such that there were fewer opportunities to obtain data on the nightside inside 10 R_S, with most of the coverage being restricted to distances greater than 5 R_S. As can be seen from Figure 5, the probability of detecting ESWs is actually highest at the closer distances to Saturn on the nightside. The orbits in 2004, 2005, and 2008 were more favorable in this regard.

5. Summary and Discussion

We have carried out an analysis of the bipolar-type ESWs observed in Cassini RPWS WBR data at distances less than 10 R_S for the years 2004, after orbit insertion, through 2008. There are two reasons why we constrained the study by distance, years, and ESW type. The first and primary reason is that it takes a considerable amount of time for a computer routine to process all the waveform data, which are received at such high sample rates, and for someone to manually check those results for ESWs, which fit the criteria for bipolar pulses. The second reason is based on the results of a prior initial study of ESWs at Saturn by *Williams et al.* [2006] for data obtained at the end of 2004 after orbit insertion up to early 2005. That study found that ESWs were observed

primarily during Cassini's closest approaches to Saturn or one of its moons and during crossings of boundary layers such as the magnetosheath and bow shock. We specifically chose to concentrate on one of these higher ESW incidence regions, i.e., closest approaches to Saturn and its moon Enceladus, in order to reasonably contain the study since we were carrying out a multiyear survey. Third, only bipolar pulse ESWs were chosen for study since they are usually more numerous than tripolar pulse ESWs and not as prone to multiple interpretations as would be the case for monopolar pulses when using measurements from a single dipole antenna. Although the Cassini RPWS waveform receiver (WFR) is capable of two axis electric field measurements and was used in the limited *Williams et al*. [2006] Saturn study, it does not have the capability to measure pulses with extremely short time scales due to its limited bandwidth (2.5 kHz).

In our event study in section 3 we concentrated on an interesting event involving an encounter with Saturn's moon Enceladus. During the Enceladus E5 encounter on 9 October 2008, several ESWs were identified in the period leading up to the encounter, but in advance of the crossing of the dust plume close to the moon. These ESWs were similar in amplitude and time duration to those reported by *Williams et al*. [2006] during the closest approach to Saturn for the early part of the mission after orbit insertion. The ESWs that we observed during the closest approach to Enceladus, however, were several tens to over 100 mV/m in amplitude compared to only 10 mV/m for those during the Titan encounters presented by *Williams et al*. [2006]. We note that some of these higher-amplitude ESWs, which may have even higher amplitudes than measured due to obtaining only one component of the electric field, fall into the category $\delta\mathbf{E}\sim O(100\ \mathrm{mV/m})$ as was found by *Andersson et al*. [2009] as one defining characteristic for solitary waves that have measurable magnetic components parallel to B_0. Because of this and because we do not have concurrent magnetic field measurements, we cannot rule out that possibility that these higher-amplitude solitary waves are electromagnetic as opposed to electrostatic.

As to whether the higher-amplitude ESWs observed at closest approach to Saturn are associated with the environment of Enceladus as opposed to the high-density region surrounding Enceladus, we have separately examined some of the Enceladus encounters in 2008 where the WBR obtained data and ESWs were observed. Every one of them shows the same trend, i.e., during the 5–7 min surrounding closest approach as the spacecraft crosses the magnetic equator, the ESW amplitudes increase by at least 1 to 2 orders of magnitude. As previously noted, the electron density actually shows a significant depression in concert with the higher-amplitude ESWs for the event shown in Figure 3. *Farrell et al*. [2009, 2010] have also shown a similar density depression for an Enceladus encounter on 12 March 2008, while *Morooka et al*. [2011] have presented evidence that this density depletion was observed on all Enceladus encounters in 2008, including the one we presented in Figure 3. *Farrell et al*. [2009, 2010] concluded that the electron depletion was due to dust-electron absorption associated with the dust envelope that surrounds Enceladus, which modifies the plasma environment in the vicinity of the moon. Thus, the unique plasma environment surrounding Enceladus could lead to generation of ESWs with higher amplitudes than found elsewhere inside 10 R_s depending on the currents that are present and the scope and scale of the plasma modifications associated with each encounter.

Because we did not use the WFR with its much narrower bandwidth, we were unable to observe ESWs with time durations longer than about 250 μs, if they existed for this event, since the data were taken in the 80 kHz filter bandwidth mode and pulse distortions take place within the WBR for longer pulses. The *Williams et al*.'s [2006] study does not provide information about the time duration of the ESWs associated with Titan. If they are similar to those observed at Enceladus, they would not have been able to observe them with the data they used from the narrower filters. The shorter time scales afforded by the 80 kHz bandwidth filter allow us to observe ESWs on time scales closer to the electron plasma frequency, which is on the order of 20–80 kHz for this event based on the upper hybrid resonance frequency. In our favor, we were thus able to observe much shorter time scale ESWs, to tens of microseconds, than the *Williams et al*.'s [2006] study because of using the wider bandwidth of WBR. Their study was confined to the WBR 10 kHz bandwidth filter and WFR, allowing for resolution of ESWs only to as short as a few 100 μs.

With regard to the survey results presented in section 4, it was conducted for the years 2004–2008 at distances less than 10 R_s. We found that the ESWs are, for the most part observed primarily on the nightside at distances less than 10 R_s, the WBD coverage being fairly well distributed across all nightside MLTs at distances from 3 to 10 R_s. The ESWs are also observed nearly uniformly from −30° to 40°, with the exceptions of the northern10–20° range containing far more than any other latitude, and the northern 20–30° range

containing hardly any. We do not have a good explanation for the ESW local time or latitude variation. As regards the characteristics of the ESWs observed in the inner region with respect to those in the outer nightside region, we found no significant differences in either ESW amplitude or time duration for these two regions, apart from those associated with the Enceladus encounters in the inner region as highlighted in Figure 3. There is the possibility that the nightside ESWs, particularly at low latitudes, are related to processes associated with the E ring, specifically dust-plasma interactions as described by *Morooka et al*. [2011], who found an interrelationship between the E ring of charged dust and the Saturnian plasma disk.

Regarding the highest incidence of ESWs at 4–6 R_s and 22:00 MLT and northern latitudes around 10–20°, these are mostly likely associated in some way with Cassini's encounters with the E ring and its moon Enceladus. We point out, however, that most of these higher-latitude ESWs are not detected in the primary dust plume close to the moon. Furthermore, although not shown in section 4 of this paper, the probability is much higher that ESWs will be detected with the wider 80 kHz bandwidth, as opposed to 10 kHz, implying that the processes that created them are ones which occur on faster time scales more likely to be associated with electrons. This leads to the conclusion that the ESWs with much longer time scales reported by *Williams et al*. [2006] up to tens of milliseconds are most likely created out of longer time scale processes often typical of ions.

In the following we discuss some possibilities for the generation of the ESWs. With regard to the Enceladus encounter, we saw that the amplitudes of the ESWs were at least 2 orders of magnitude higher when crossing the dust plume around closest approach (19:06:40 UT) than those observed just prior to the encounter (18:15–18:40 UT). We have correlated this region of high-amplitude ESWs with the changes in magnetic field and electron density associated with the close approach to Enceladus. The *Williams et al*.'s [2006] study of ESWs from early Saturn observations found a trend for higher ESW amplitudes with higher ambient magnetic field amplitudes, similar to a trend found at Earth by *Pickett et al*. [2004b]. This trend is consistent with the key property of BGK solitary waves whose widths and potential amplitudes are constrained [*Chen et al*., 2004] and thus provides some basis for the possibility that these ESWs are BGK mode phase space holes. However, as noted in the introduction, depending on the width of the soliton and the parametric range used [*Ghosh and Lakhina*, 2004], the amplitudes of the solitons obtained by the Sagdeev pseudopotential techniques can either increase or decrease depending on the width of the soliton. Thus, the ESW amplitude-magnetic field amplitude trend could likewise be supportive of these ESWs being solitons created out of an acoustic instability.

Based on an analysis of the Cassini CAPS [*Young et al*., 2004] data showing the absence of electron or ion beams during the closest approach to Enceladus (~19:06–19:08 UT) and during the earlier period of 18:15–18:40 UT even after subtracting out the penetrating radiation, we can probably rule out local generation at the spacecraft due to any type of acoustic or beam instability, including the Buneman mode. However, due to the current system induced by the interaction of the magnetospheric plasma of Saturn with the atmospheric plume of the icy moon Enceladus, we conclude that a current instability cannot be ruled out for the local creation of the ESWs seen in connection with the Enceladus encounter.

The *Williams et al*.'s [2006] study found an increased observation rate of ESWs in association with close encounters with Titan at 20 R_s in 2004 and even more so during a 2 h period of time shortly after periapsis. For the period shortly after periapsis they speculated that the spacecraft was moving through a current system induced by an interaction between the corotating plasma and the Saturn rings due to the presence of auroral hiss at the time. During an Enceladus encounter on 21 November 2009, *Gurnett et al*. [2011] attributed the ramp-like variations of the measured magnetic field seen near closest approach to the moon as nearly field-aligned currents associated with a standing shear-mode Alfvén wave excited by the moon, similar to a process at Jupiter's moon, Io. Further, *Simon et al*. [2014] specifically state that for the E5 9 October 2008 event studied here and several other Enceladus encounters, the magnetic field is discontinuous at the surface of the Enceladus flux tube and these flux tubes are purely rotational. Thus, the ramp-like variations in the magnetic field seen during the 9 October 2008 Enceladus encounter may provide the necessary currents to generate ESWs. Also, the density cavity observed at closest approach is similar to those observed in Earth's upward and downward auroral current regions. It is typical for ESWs to be generated in this region on the edges of these density cavities or within small-scale density enhancements within the cavity [*Pottelette et al*., 2014]. Thus, the presence of ESWs associated with the density cavity and current system near closest approach to Enceladus might tend to favor local generation of ESWs through a current instability.

Similar to our situation here, the *Malaspina et al.*'s [2013] study of ESWs observed in the solar wind found no evidence of beam or Buneman-type instabilities, but the ESWs were associated with magnetic current sheets. They concluded that an instability capable of producing ESWs was active at current sheets in the solar wind at 1 AU and that such an instability might indicate the conversion of magnetic energy into plasma kinetic energy localized to solar wind current sheets, a process suggested by turbulence studies.

Given that solitary waves can propagate from their source region, beam and acoustic instabilities are viable for the creation of the ESWs reported in this study but they will not have been generated in situ. We base this conclusion on the report of electron beams being observed in connection with auroral hiss funnels near Enceladus [*Gurnett et al*., 2011]. *Leisner et al*. [2013] further investigated the presence of auroral hiss with magnetic field aligned electron beams. They found that auroral hiss emissions were present during 7 of 20 Enceladus encounters, these seven including all of the non-high-inclination flybys through the Enceladus flux tube. The event we discuss, E5, was not one of those seven, implying that electron beams may not be expected for this flyby. However, this may simply be a matter of not crossing the Enceladus flux tube at the active location where beams are present and ESWs and auroral hiss are generated. Therefore, the absence of electron beams in situ does not necessarily rule out their generation by typical beam and acoustic instabilities. It may also be possible that some of the ESWs are created out of dust acoustic instabilities as discussed for dusty plasmas such as Saturn's E rings [e.g., *Alinejad*, 2010; *Shukla and Eliasson*, 2012; *Akhter et al*., 2013].

It is beyond the scope of this paper to further pursue the specifics of the generation mechanisms discussed above for generating the ESWs observed near Saturn and Enceladus. Rather, we leave that investigation to modelers and theorists.

Acknowledgments

The research carried out at the University of Iowa was supported by JPL contract 1415150. G.H.J. is partly supported by the UK Science and Technology Facilities Council. We acknowledge Michele Dougherty and the Planetary Data System for the MAG data shown in this paper. We thank L.-J. Chen for supporting WBR test data. We also acknowledge helpful discussions with S.-Y. Ye and G. Hospodarsky and supporting data provided by J. Groene. We particularly acknowledge J.D. Williams for access to the software detection routines used to carry out the study. J.S.P. and R.L.H. thank Rick and Pat McCann for IT services and support. All data used in this study are available through the public Planetary Data System and from the authors at the University of Iowa.

M. Balikhin thanks Forrest Mozer and another reviewer for their assistance in evaluating this paper.

References

Akhter, T., A. Mannan, and A. A. Mamun (2013), Dust acoustic solitary waves in a four component adiabatic magnetized dusty plasma, *Plasma Phys. Rep.*, *39*(7), 548–555, doi:10.1134/S1063780X13070015.

Alinejad, H. (2010), Dust ion-acoustic solitary and shock waves in a dusty plasma with non-thermal electrons, *Astrophys. Space Sci.*, *327*, 131–137, doi:10.1007/s10509-010-0296-z.

Andersson, L., et al. (2009), New features of electron phase space holes observed by the THEMIS mission, *Phys. Rev. Lett.*, *102*, 225004, doi:10.1103/PhysRevLett.102.225004.

Bernstein, I. B., J. M. Greene, and M. D. Kruskal (1957), Exact nonlinear plasma oscillations, *Phys. Rev. Lett.*, *108*, 546–550.

Chen, L.-J., and G. K. Parks (2002), BGK electron solitary waves in 3D magnetized plasma, *Geophys. Res. Lett.*, *29*(9), 1331, doi:10.1029/2001GL013385.

Chen, L.-J., D. J. Thouless, and J.-M. Tang (2003), Width-amplitude relation of Bernstein-Greene-Kruskal solitary waves. [Available at http://arxiv.org/abs/physics/0303021.]

Chen, L.-J., D. J. Thouless, and J.-M. Tang (2004), Bernstein-Greene-Kruskal solitary waves in three-dimensional magnetized plasma, *Phys. Rev. E*, *69*, 055402(R).

Dougherty, M. K., et al. (2004), The Cassini magnetic field investigation, *Space Sci. Rev.*, *114*, 331–383.

Dougherty, M. K., K. K. Khurana, F. M. Neubauer, C. T. Russell, J. Saur, J. S. Leisner, and M. E. Burton (2006), Identification of a dynamic atmosphere at Enceladus with the Cassini magnetometer, *Science*, *311*, 1406–1409, doi:10.1126/science.1120985.

Dubouloz, N., R. Pottelette, M. Malingre, and R. A. Treumann (1991), Generation of broadband electrostatic acoustic solitons, *Geophys. Res. Lett.*, *18*, 155–158, doi:10.1029/90GL02677.

Ergun, R. E., et al. (1998a), FAST satellite observations of large-amplitude solitary structures, *Geophys. Res. Lett.*, *25*(12), 2041–2044, doi:10.1029/98GL00636.

Ergun, R. E., C. W. Carlson, J. P. McFadden, F. S. Mozer, L. Muschietti, I. Roth, and R. Strangeway (1998b), Debye-scale plasma structures associated with magnetic-field-aligned electric fields, *Phys. Rev. Lett.*, *81*, 826.

Farrell, W. M., W. S. Kurth, D. A. Gurnett, R. E. Johnson, M. L. Kaiser, J.-E. Wahlund, and J. H. Waite Jr. (2009), Electron density dropout near Enceladus in the context of water-vapor and water-ice, *Geophys. Res. Lett.*, *36*, L10203, doi:10.1029/2008GL037108.

Farrell, W. M., W. S. Kurth, R. L. Tokar, J.-E. Wahlund, D. A. Gurnett, Z. Wang, R. J. MacDowell, M. W. Morooka, R. E. Johnson, and J. H. Waite Jr. (2010), Modification of the plasma in the near-vicinity of Enceladus by the enveloping dust, *Geophys. Res. Lett.*, *37*, L20202, doi:10.1029/2010GL044768.

Franz, J. R., P. M. Kintner, and J. S. Pickett (1998), POLAR observations of coherent electric field structures, *Geophys. Res. Lett.*, *25*, 1277–1280, doi:10.1029/98GL50870.

Franz, J. R., P. M. Kintner, J. S. Pickett, and L.-J. Chen (2005), Properties of small-amplitude electron phase-space holes observed by Polar, *J. Geophys. Res.*, *110*, A09212, doi:10.1029/2005JA011095.

Ghosh, S. S., and G. S. Lakhina (2004), Anomalous width variation of rarefactive ion acoustic solitary waves in the context of auroral plasmas, *Nonlinear Processes Geophys.*, *11*, 219–228.

Gurnett, D. A. (1975), The Earth as a radio source: The non-thermal continuum, *J. Geophys. Res.*, *80*, 2751–2763, doi:10.1029/JA080i019p02751.

Gurnett, D. A., and L. A. Frank (1977), A region of intense plasma wave turbulence on auroral field lines, *J. Geophys. Res.*, *82*, 1031–1050, doi:10.1029/JA082i007p01031.

Gurnett, D. A., L. A. Frank, and R. P. Lepping (1976), Plasma waves in the distant magnetotail, *J. Geophys. Res.*, *81*, 6059–6071, doi:10.1029/JA081i034p06059.

Gurnett, D. A., et al. (2004), The Cassini radio and plasma wave investigation, *Space Sci. Rev.*, *114*, 395–463.

Gurnett, D. A., et al. (2011), Auroral hiss, electron beams and standing Alfvén wave currents near Saturn's moon Enceladus, *Geophys. Res. Lett.*, *38*, L06102, doi:10.1029/2011GL046854.

Hansen, C. J., L. W. Esposito, A. I. F. Stewart, J. E. Colwell, A. R. Hendrix, W. Pryor, D. Shemansky, and R. West (2006), Enceladus' water vapor plume, *Science*, *311*, 1422–1425.

Hashimoto, K., et al. (2010), Electrostatic solitary waves associated with magnetic anomalies and wake boundary of the Moon observed by KAGUYA, *Geophys. Res. Lett.*, *37*, L19204, doi:10.1029/2010GL044529.

Jones, G. H., et al. (2009), Fine jet structure of electrically charged grains in Enceladus' plume, *Geophys. Res. Lett.*, *36*, L16204, doi:10.1029/2009GL038284.

Kurth, W. S., D. A. Gurnett, and R. R. Anderson (1981), Escaping nonthermal continuum radiation, *J. Geophys. Res.*, *86*, 5519–5531, doi:10.1029/JA086iA07p05519.

Kurth, W. S., D. A. Gurnett, A. M. Persoon, A. Roux, S. J. Bolton, and C. J. Alexander (2001a), The plasma wave environment of Europa, *Planet. Space Sci.*, *49*, 345–363.

Kurth, W. S., G. B. Hospodarsky, D. A. Gurnett, M. L. Kaiser, J.-E. Wahlund, A. Roux, P. Canu, P. Zarka, and Y. Tokarev (2001b), An overview of observations by the Cassini radio and plasma wave investigation at Earth, *J. Geophys. Res.*, *106*, 30,239–30,252, doi:10.1029/2001JA900033.

Lakhina, G. S., S. V. Singh, A. P. Kakad, and J. S. Pickett (2011), Generation of electrostatic solitary waves in the plasma sheet boundary layer, *J. Geophys. Res.*, *116*, A10218, doi:10.1029/2011JA016700.

Lee, N., et al. (2012), Measurements of freely-expanding plasma from hypervelocity impacts, *Int. J. Impact Eng.*, *44*, 40–49, doi:10.1016/j.ijimpeng.2012.01.002.

Lefebvre, B., L.-J. Chen, W. Gekelman, P. Kintner, J. Pickett, P. Pribyl, and S. Vincena (2011), Debye-scale solitary structures measured in a beam-plasma laboratory experiment, *Nonlinear Processes Geophys.*, *18*, 41–47, doi:10.5194/npg-18-41-2011.

Leisner, J. S., G. B. Hospodarsky, and D. A. Gurnett (2013), Enceladus auroral hiss observations: Implications for electron beam locations, *J. Geophys. Res. Space Physics*, *118*, 160–166, doi:10.1029/2012JA018213.

Li, S. Y., Y. Omura, B. Lembège, X. H. Deng, H. Kojima, Y. Saito, and S. F. Zhang (2014), Geotail observation of counter directed ESWs associated with the separatrix of magnetic reconnection in the near-Earth magnetotail, *J. Geophys. Res. Space Physics*, *119*, 202–210, doi:10.1002/2013JA018920.

Malaspina, D. M., D. L. Newman, L. B. Wilson III, K. Goetz, P. J. Kellogg, and K. Kerstin (2013), Electrostatic solitary waves in the solar wind: Evidence for instability at solar wind current sheets, *J. Geophys. Res. Space Physics*, *118*, 591–599, doi:10.1002/jgra.50102.

Malaspina, D. M., L. Andersson, R. E. Ergun, J. R. Wygant, J. W. Bonnell, C. Kletzing, G. D. Reeves, R. M. Skoug, and B. A. Larsen (2014), Nonlinear electric field structures in the inner magnetosphere, *Geophys. Res. Lett.*, *41*, 5693–5701, doi:10.1002/2014GL061109.

Matsumoto, H., H. Kojiima, T. Miyatake, Y. Omura, M. Okada, I. Nagano, and M. Tsutsui (1994), Electrostatic solitary waves (ESW) in the magnetotail: BEN wave forms observed by Geotail, *Geophys. Res. Lett.*, *21*, 2915–2918, doi:10.1029/94GL01284.

Morooka, M. W., J.-E. Wahlund, M. Shafiz, W. M. Farrell, D. A. Gurnett, W. S. Kurth, A. M. Persoon, M. Andre, A. I. Ericksson, and M. Holmberg (2011), Dusty plasma in the vicinity of Enceladus, *J. Geophys. Res.*, *116*, A12221, doi:10.1029/2011JA017352.

Mozer, F. S., R. Ergun, M. Temerin, C. Cattell, J. Dombeck, and J. Wygant (1997), New features of time domain electric-field structures in the auroral acceleration region, *Phys. Rev. Lett.*, *79*, 1281.

Mozer, F. S., S. D. Bale, J. W. Bonnell, C. C. Chaston, I. Roth, and J. Wygant (2013), Megavolt parallel potentials arising from double-layer streams in the Earth's outer radiation belt, *Phys. Rev. Lett.*, *111*, 2335002, doi:10.1103/PhysRevLett.111.235002.

Mozer, F. S., O. Agapitov, V. Krasnoselskikh, S. Lejosne, G. D. Reeves, and I. Roth (2014), Direct observation of radiation-belt electron acceleration from electron-volt energies to megavolts by nonlinear whistlers, *Phys. Rev. Lett.*, *113*, 035001, doi:10.1103/PhysRevLett.113.035001.

Pickett, J. S., et al. (2004a), Solitary waves observed in the auroral zone: The Cluster multi-spacecraft perspective, *Nonlinear Processes Geophys.*, *11*, 183–196.

Pickett, J. S., L.-J. Chen, S. W. Kahler, O. Santolik, D. A. Gurnett, B. T. Tsurutani, and A. Balogh (2004b), Isolated electrostatic structures observed throughout the Cluster orbit: Relationship to magnetic field strength, *Ann. Geophys.*, *22*, 2515–2523, doi:10.5194/angeo-22-2515-2004.

Pickett, J. S., et al. (2005), On the generation of solitary waves observed by Cluster in the near-Earth magnetosheath, *Nonlinear Processes Geophys.*, *12*, 321–336.

Pickett, J. S., et al. (2010), On the propagation and modulation of electrostatic solitary waves observed near the magnetopause on Cluster, in *Modern Challenges in Nonlinear Plasma Physics: A Festchrift Honoring the Career of K. Papadopoulos*, *AIP Conf. Proc.*, vol. 1320, edited by D. Vassiliadis et al., Am. Inst. of Physics, Melville, New York.

Pottelette, R., M. Berthomier, and J. Pickett (2014), Radiation in the neighbourhood of a double layer, *Ann. Geophys.*, *32*, 677–687, doi:10.5194/angeo-32-677-2014.

Shukla, P. K., and B. Eliasson (2012), Nonlinear dynamics of large-amplitude dust acoustic shocks and solitary pulses in dusty plasmas, *Phys. Rev. E*, *86*, 046402, doi:10.1103/PhysRevE.86.046402.

Simon, S., J. Saur, S. C. van Treeck, H. Kriegel, and M. K. Dougherty (2014), Discontinuities in the magnetic field near Enceladus, *Geophys Res. Lett.*, *41*, 3359–3366, doi:10.1002/2014GL060081.

Spahn, F., et al. (2006), Cassini dust measurements at Enceladus and implications for the origin of the E ring, *Science*, *311*, 1416.

Swanner, J. M., J. S. Pickett, J. R. Phillips, D. L. Kirchner (2006), WBD response to bipolar and tripolar pulses: bench tests vs. in flight observations. [Available at http://caa.estec.esa.int/documents/teams/WBD/pulse_tests.pdf.]

Temerin, M., K. Cerny, W. Lotko, and F. S. Mozer (1982), Observations of double layers and solitary waves in the auroral plasma, *Phys. Rev. Lett.*, *48*, 1175–1179.

Tsurutani, B., J. Arballo, G. Lakhina, C. Ho, B. Buti, J. Pickett, and D. Gurnett (1998), Plasma waves in the dayside polar cap boundary layer: Bipolar and monopolar electric pulses and whistler mode waves, *Geophys. Res. Lett.*, *25*, 4117, doi:10.1029/1998GL900114.

Williams, J. D., L.-J. Chen, W. S. Kurth, D. A. Gurnett, M. K. Dougherty, and A. M. Rymer (2005), Electrostatic solitary structures associated with the November 10, 2003, interplanetary shock at 8.7 AU, *Geophys. Res. Lett.*, *32*, L17103, doi:10.1029/2005GL023079.

Williams, J. D., L.-J. Chen, W. S. Kurth, D. A. Gurnett, and M. K. Dougherty (2006), Electrostatic solitary structures observed at Saturn, *Geophys. Res. Lett.*, *33*, L06103, doi:10.1029/2005GL024532.

Ye, S.-Y., D. A. Gurnett, W. S. Kurth, T. F. Averkamp, M. Morooka, S. Sakai, and J.-E. Wahlund (2014), Electron density inside Enceladus plume inferred from plasma oscillations excited by dust impacts, *J. Geophys. Res. Space Physics*, *119*, 3373–3380, doi:10.1002/2014JA019861.

Young, D., et al. (2004), Cassini Plasma Spectrometer investigation, *Space Sci. Rev.*, *114*, 1–112, doi:10.1007/s11214-004-1406-4.